

Chapter 5

BUCKLING LOAD OF GRID SHELLS WITH VARIOUS CONNECTION SYSTEMS AND DIFFERENT RISE-SPAN RATIOS

In order to investigate the influence of various connecting systems on the buckling load of global shallow grid shells, stability analysis were performed in this chapter. Using all of the moment-rotation curves and load displacement curves which were performed in chapter 4, buckling behaviors could be simulated with special consideration to the nonlinear connection stiffness of various connection systems, in particular, the deviations of bolt-holes, namely bolt clearances (ΔV), with various rise-span ratios of the global grid shells.

5.1 Geometrical details

As shown in Figure 5.1, the three-way grid shells with a span of 25 m and 50 m were simulated using three different ratios of rise (f) to span (d) as 0.1(a), 0.2(b) and 0.3(c) to find out the overall behavior of the global grid shells with different rise-span ratios (f/d) and ΔV (Table 5.1 and 5.2). Recently, the three-way grid is often being used in shallow single-layer grid shells and free-form spatial grid shells. Thus, this research adopted this type of three-way grid for the global simulations.

5.2 Finite element model

Figure 5.3 shows the elements that were used in the finite element model. To consider both geometric and material nonlinearities in the grid shell with a semi-rigid connection, three nonlinear spring elements of COMBIN39, which were supported by a specific function of ANSYS, were implemented to simulate connection stiffness. This element is a nonlinear spring element which has a unidirectional de-

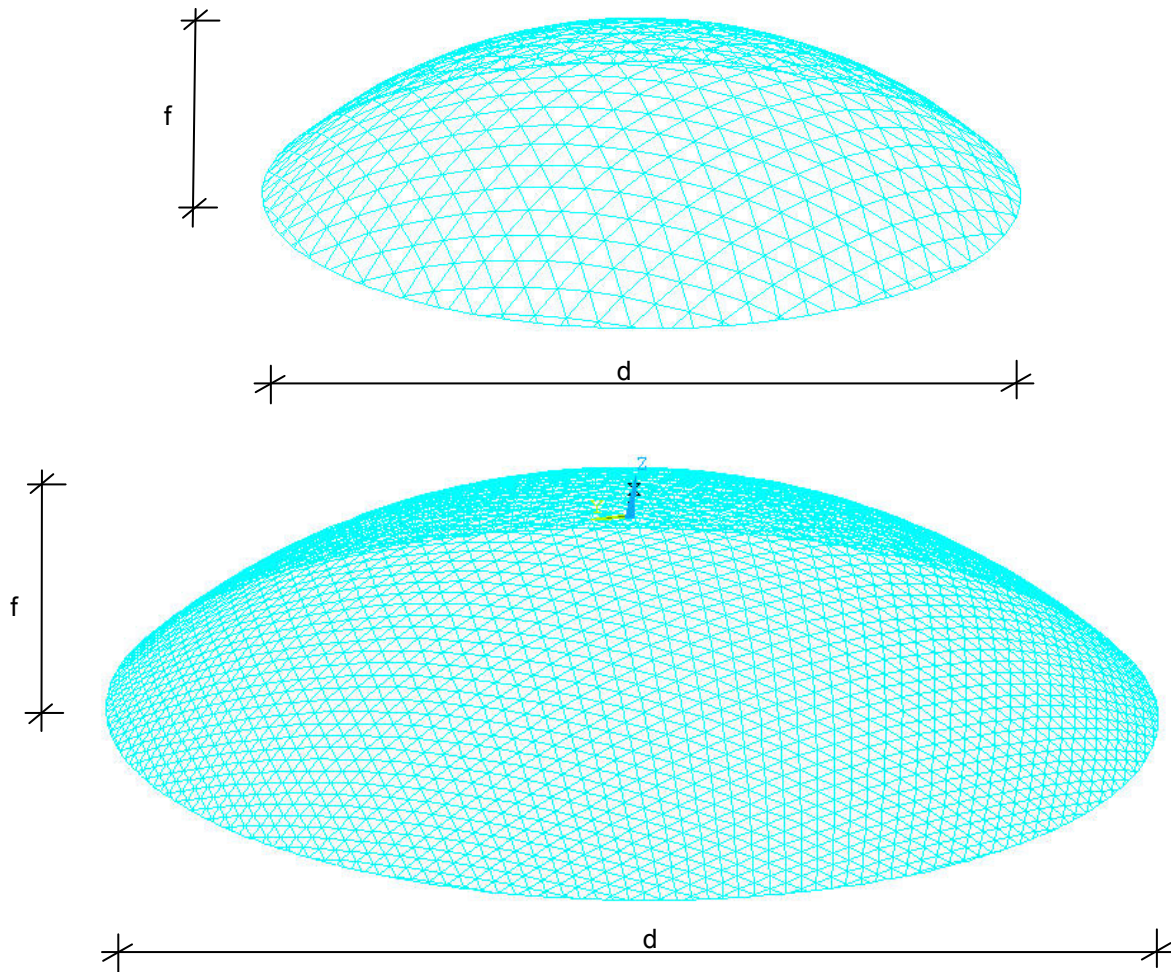


Figure 5.1: Models of three-way grid shells, 25 m (above) and 50 m (below)

Table 5.1: Values of grid shell 25m

Grid shells (f/d)	25-25-2.5 (0.1)	25-25-5 (0.2)	25-25-7.5 (0.3)
High (f) [m]	2.5	5.0	7.5
Span (d) [m]	25		
Member	L=1.2 m, b×h=60mm×60mm, S355		
Boundary condition	Rigid support		

Table 5.2: Values of grid shell 50m

Grid shells (f/d)	50-50-5 (0.1)	50-50-10 (0.2)	50-50-15 (0.3)
High (f) [m]	5	10	15
Span (d) [m]	50		
Member	L=1.2 m, b×h=60mm×60mm, S355		
Boundary condition	Rigid support		

gree of freedom. In this analysis, the bending stiffness (M_y and M_z) and axial force (F) could be simulated by inputting the real constants of COMBIN39 through a local coordination, because the spatial location of every element in the structural model is different. Thus a local coordinate system is necessary to ensure the physical meaning of spring element according to the coordination of every element. The center of node and beam were simulated by BEAM188 which is a quadratic beam element in 3-dimension with six degrees of freedom at each node [ANSYS v11 2009] and the node was assumed to be a rigid one [Ma et al 2009].

The nonlinear spring element of COMBIN39 has not yet been commonly used for the node stiffness in the analysis for 3-dimensional spatial structures. However, in the field of beam-to-column connectors for the steel frame, the COMBIN39 has been very often adopted to simulated their nonlinear stiffness of connector [Bajoria et al 2006]. Nevertheless, some research, which investigated global spatial structures, have adopted COMBIN39 element nowadays. For instance, H. H. Ma (2008) converted nonlinear stiffness of bolt-ball connection system to COMBIN39 and simulated a single layer K8 dome to figure out the buckling behaviors with nonlinear stiffness of semi-rigid bolt-ball connections [Ma et al 2009].

5.3 Material properties

The material of the beam member was assumed to be steel S355 with E-Module 210000 N/mm². The cross section was $b \times h = 60\text{mm} \times 60\text{mm}$ and the maximum length of beam (L) was 1.20 m. It was also assumed that the structures are covered with the glass panels. The glass panels were not performed in a structural sense but the dead load was just transferred to the concentrated load in the node. For the boundary condition, the rigid support was adopted. The dead load (g) of steel beam was $\gamma = 78.5 \text{ kN/m}^3$ and 20 mm thickness of glass glazing ($\gamma_g = 25 \text{ kN/m}^3$) was calcula-

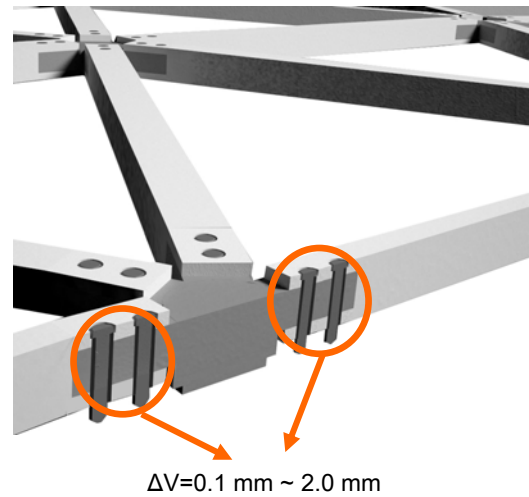


Figure 5.2: Graphic assuming of different bolt clearances in the connection of global grid shells

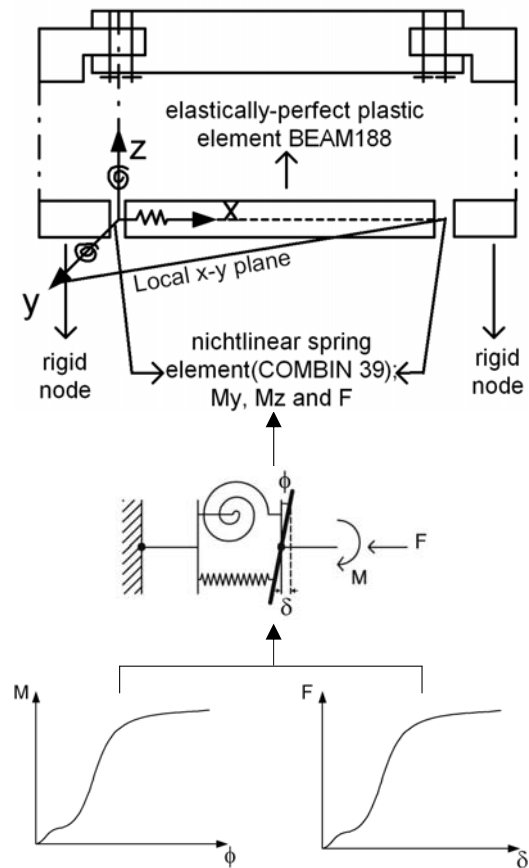


Figure 5.3: Finite element applied in grid shell

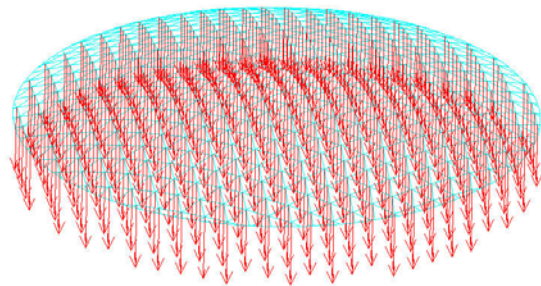
ted as well. As for the live load, a snow load (s) of 0.75 kN/m² was applied to the structure and all of the load was transferred as nodal load.

To obtain a critical point in the load-carrying characteristic of the grid shell, the load control method was performed. According to the German standard DIN 18800, the design load factor (p) was incremented from $p=1.35g+1.5s$ corresponding to loading factor 1.0 [Knippers et al 1997] [Bulenda et al 2005]. Concerning the load case, a symmetrical load case $g+s$ (dead load + snow load) and asymmetrical load case $g+s/2$ (dead load + snow on half of the structure) were applied to the structures (Figure 5.4).

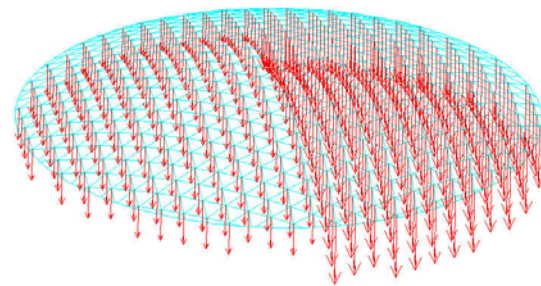
All of the critical failure was assumed to have occurred in the global buckling, with the assumption that no member buckling took place, in order to find out the influence of connection stiffness on global instability behavior. For that the strength of cross section was checked through a postprocessor using the condition of plastic flow method [Bulenda et al 1999] [Bulenda et al 2005]:

$$\frac{M_{y_i}}{M_{y,pl,d}} + \frac{M_{z_i}}{M_{z,pl,d}} + \left(\frac{N_i}{N_{pl,d}} \right)^2 \leq 1 \quad (5.1)$$

with N_i , M_{y_i} and M_{z_i} : internal forces from the elastic computation and $N_{pl,d}$, $M_{y,pl,d}$ and $M_{z,pl,d}$: full capacities of members.



(a) symmetrical load case (g+s)



(b) asymmetrical load case (g+s/2)

Figure 5.4: Two load cases

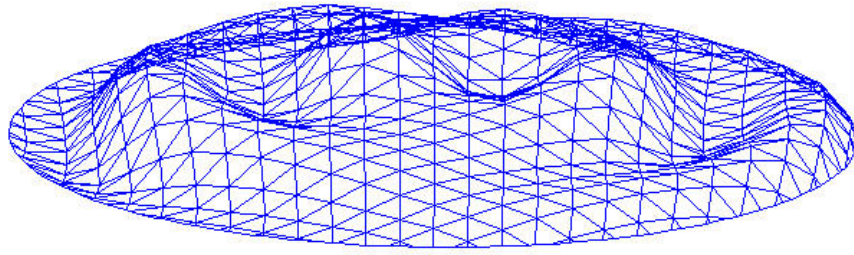
5.4 Geometrical initial imperfection

The stability failure of a structure occurs with a sudden structural change of loading path which causes a low load-bearing capacity of the shell. Many reasons can be given for that. Among these reasons, most important being, geometrical initial imperfections, such as a mismatch of member section or a non-accurate assembling of structure, can bring a crucial influence of the load-bearing capacity of the shell [Ei Naschie 1990] [Blandini 2005]. To provide appropriate structural solutions for this problem, a lot of researches have reported initial imperfection on the global shell. However, it is not simple to predict which kind of imperfection may lead to the lowest buckling load on grid a shell.

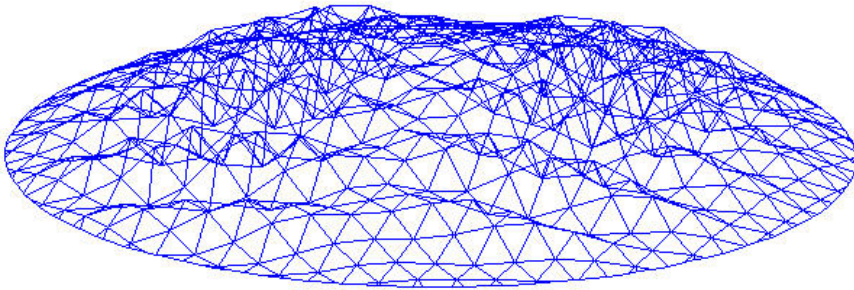
Thus, in this study, the initial geometrical imperfection vector was obtained by [Bulenda et al 2005] [Knippers et al 1997]

- the perfect structures were chosen without any imperfection as a reference structure;
- the deformation's shapes were obtained by a linear computation through the symmetrically loaded structure (dead load and snow load on the entire structure);
- imperfection vectors could be gained by linear combinations of eigenvectors based on the lowest eigenvalues at the critical point of the load-displacement curves.

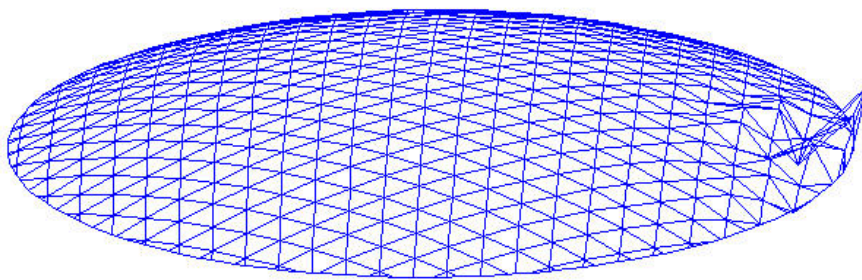
In terms of the size of the imperfection vector, to apply a realistic scaling of imperfection value, the buckling mode of structure was observed after the eigenmode computation. If the model shows a global buckling mode, long wave displacements could be obtained and it did make sense to use the maximum value of the imperfection ratio of the span d , for example 0.1% of d . Once a local buckling mode was found, the general difference of displacements between buckled node and non-buckled node was already large, with the large size of the imperfection far away from realistic scaling. Thus, in this case, the imperfection's size



(a) Rigid connection
(Imperfection size: 0.1% of d)

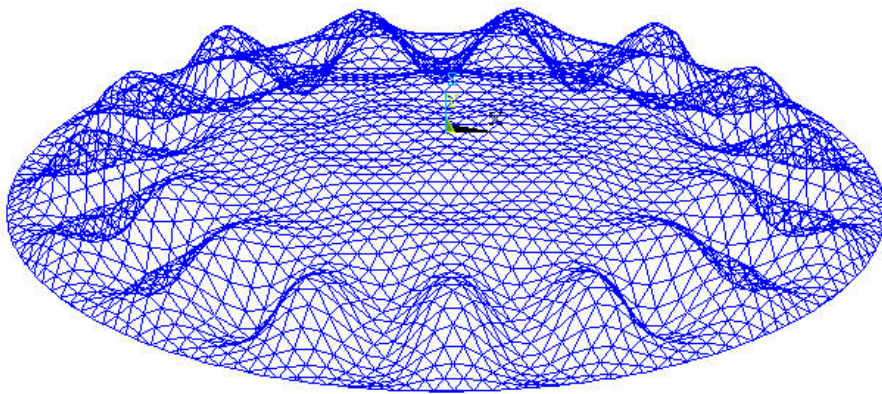


(b) Connection system 2
(Imperfection size: 0.01% of d)

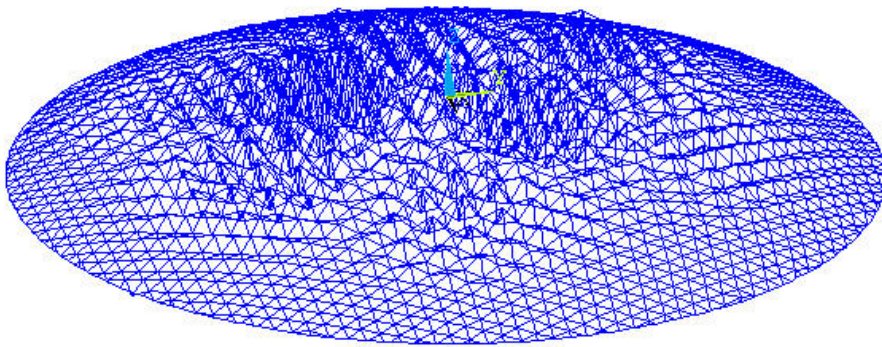


(c) Connection system 4
(Imperfection size: 0.01% of d)

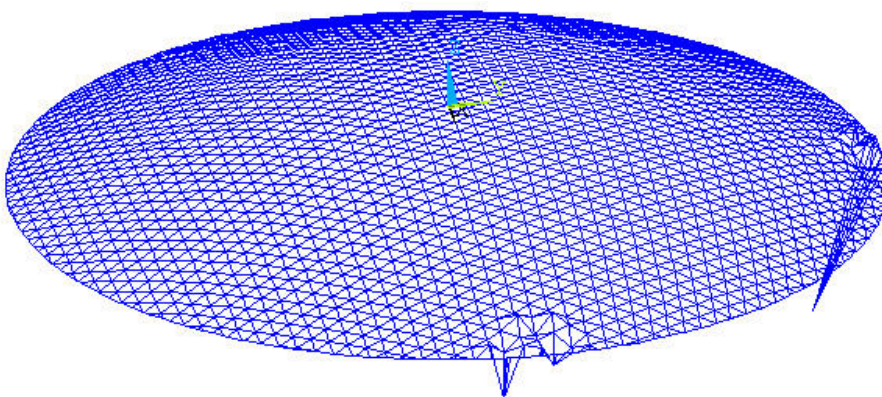
Figure 5.5: The first eigenmode of grid shells - $f=25$ m ($f/d=0.1$) ($\Delta V=2.0$ mm), superelevation 200 times



(a) Rigid connection
(Imperfection size: 0.1% of d)



(b) Connection system 2
(Imperfection size: 0.01% of d)



(c) Connection system 4
(Imperfection size: 0.01% of d)

Figure 5.6: The first eigenmode of grid shells - $f=50$ m ($f/d=0.1$) ($\Delta V=2.0$ mm), superelevation 200 times

was calibrated by smaller size of scaling than the global buckling's one, e.g. 0.01% of span d . Consequently, the maximal scaling of 50 mm was sized to the node in the z -coordination as adopted in the similar reference [Bulenda et al 2005].

5.5 Investigations of parameter study

5.5.1 The influence of rise-span ratio with connection stiffness on buckling load

Based on the moment-rotation and load-displacement curves of four node connections from chapter 4, the global grid shells were investigated with three rise-span ratios ($f/d=0.1, 0.2$ and 0.3). Figure 5.5 and 5.6 show the first eigenmode of $f/d=0.1$ of grid shells 25 m and 50 m, respectively. To represent the influence of different connection stiffness on buckling behavior and rigid connection, connection system 2 and 4 are introduced here. As mentioned in chapter 4, general connection stiffness of connection system 2 showed higher than system 4. Moreover, connection stiffness of system 4 with $\Delta V=2.0$ mm was the lowest among four systems except for the bending stiffness M_z . Therefore, it could be easily expected that various buckling modes could be observed by these three connection systems.

As shown in these figures, the first eigenmode's shapes with various connection types are different. The shape of a rigid connection of grid shells presents a typical global buckling behavior. Figure 5.5(c) and 5.6(c) shows the first eigenmode shape with connection system 4. Because the nodal stiffness is weak, the buckling behavior shows a tendency toward a local failure around the boundary so that the buckling can occur easily by increasing the load. This shape is quite similar other reported literatures [Bulenda et al 2005] [Ueki et al 1991]. And it can also be predicted that the failure load factor would be lower than the one of connection system 2. All the shapes of these buckling modes will provide for shapes of imperfection analysis in the next step.

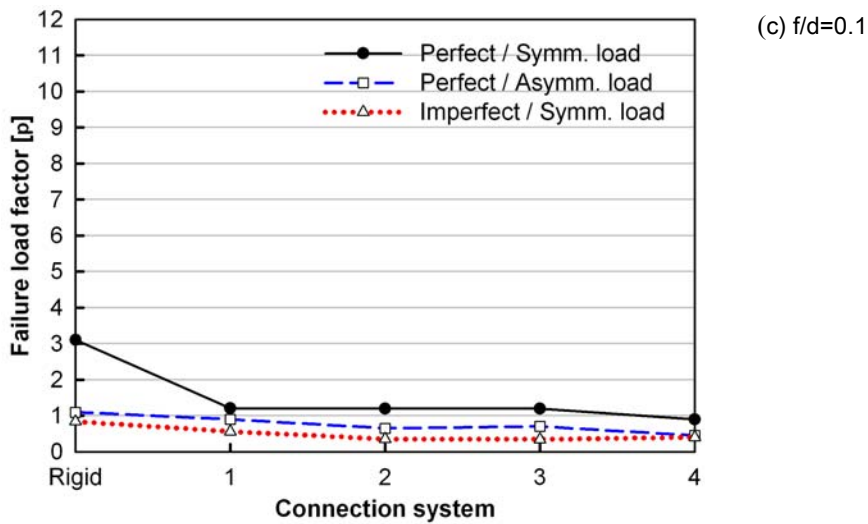
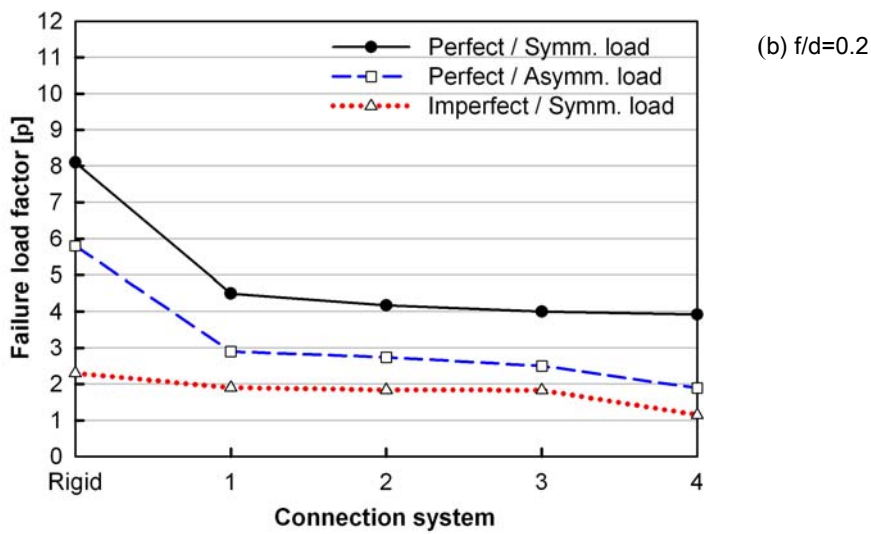
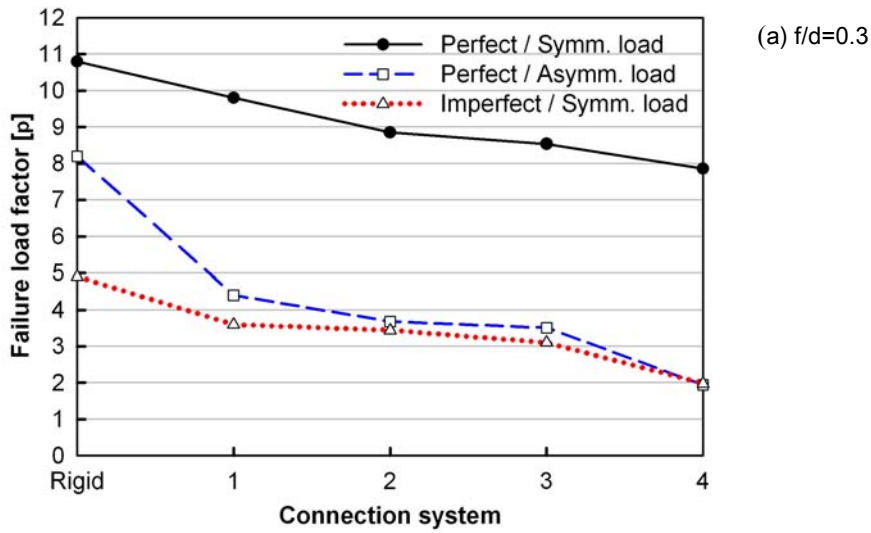


Figure 5.7:
Failure load factor (p) - f/d and various connection systems, $f=25$ m ($\Delta V=2.0$ mm)

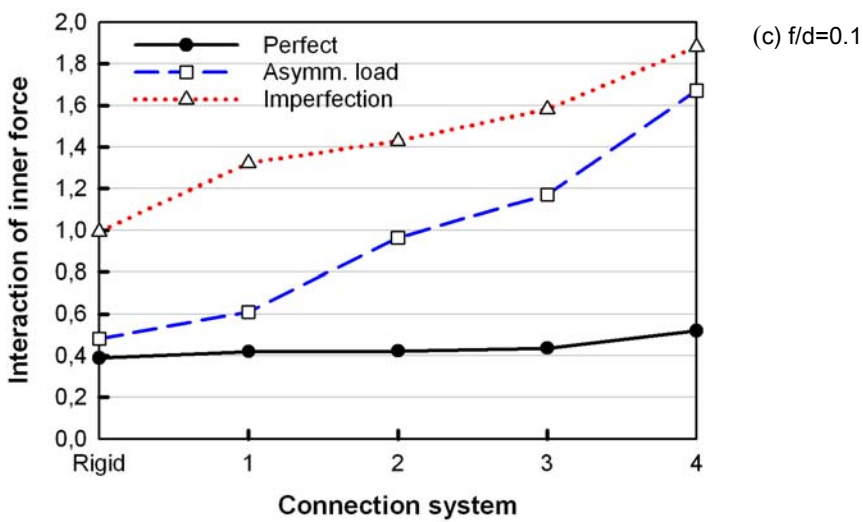
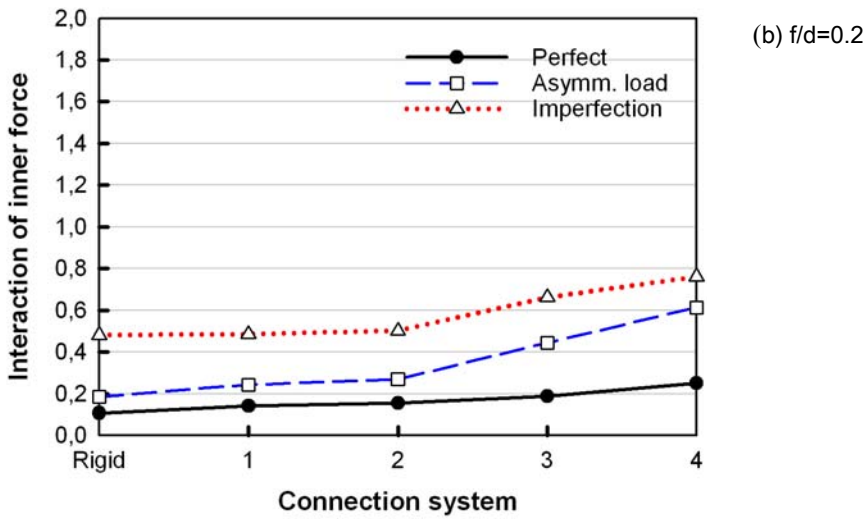
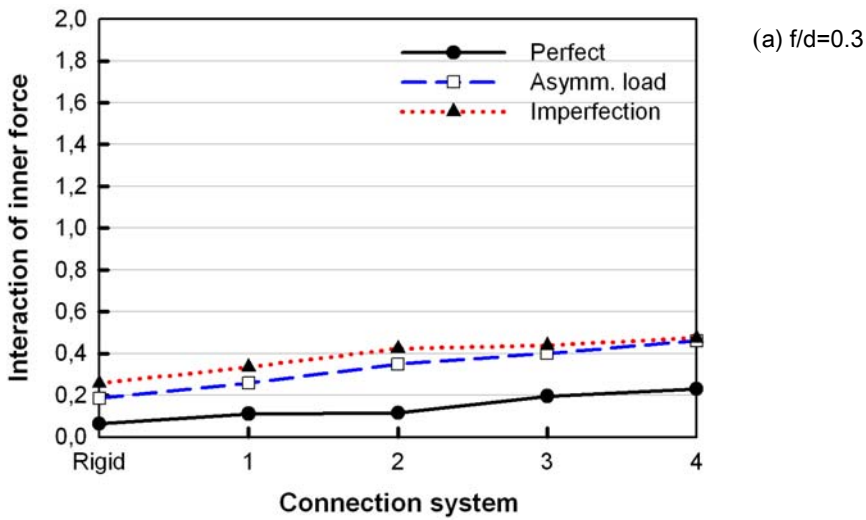


Figure 5.8:
Interaction of inner forces - f/d and various connection systems,
 $f=25\text{ m}$ ($\Delta V=2.0\text{ mm}$)

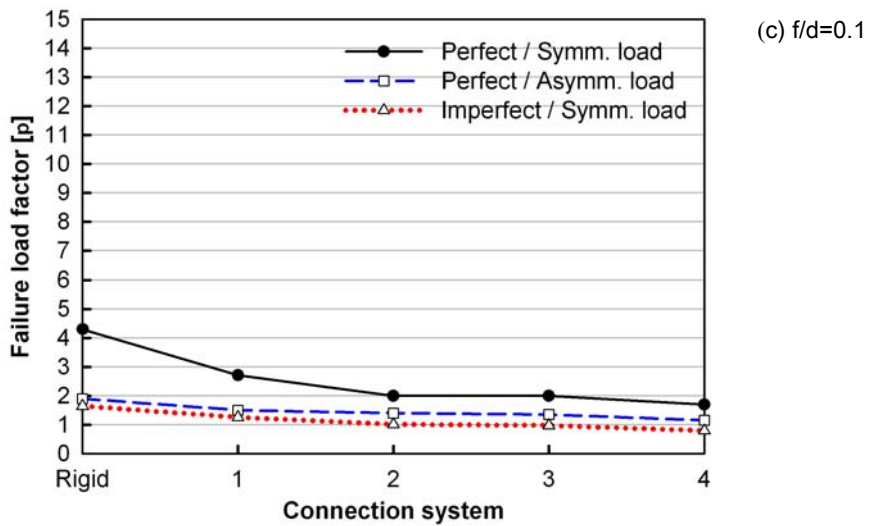
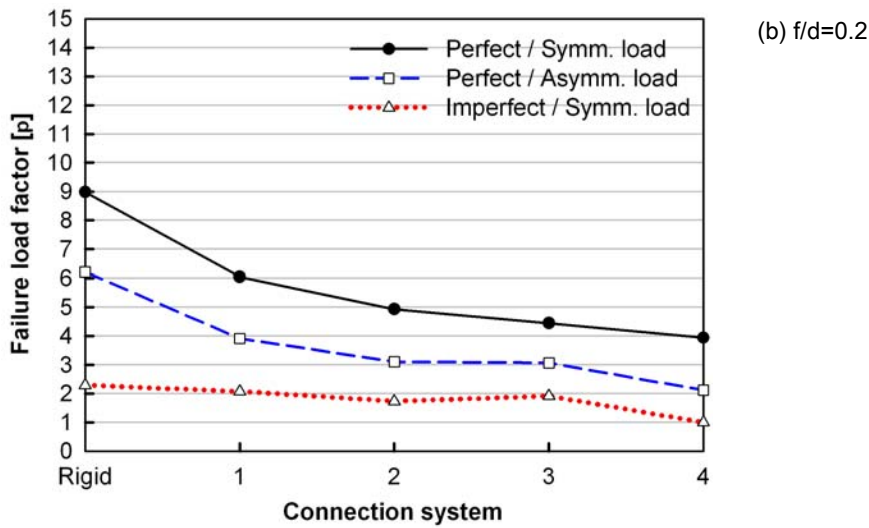
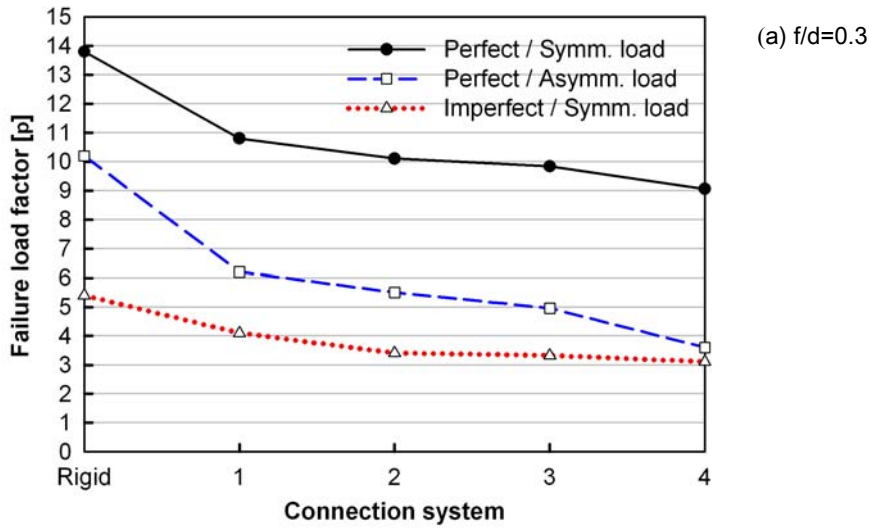


Figure 5.9:
Failure load factor (p) - f/d and various connection systems, $f=50$ m ($\Delta V=2.0$ mm)

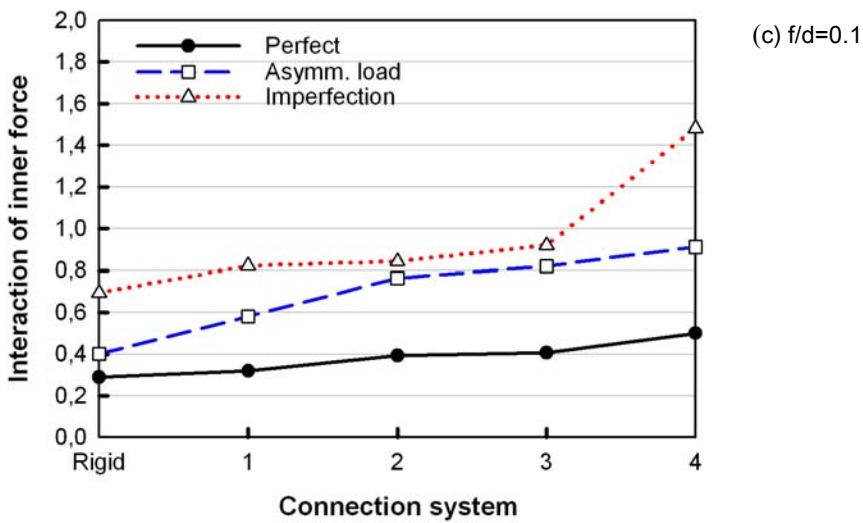
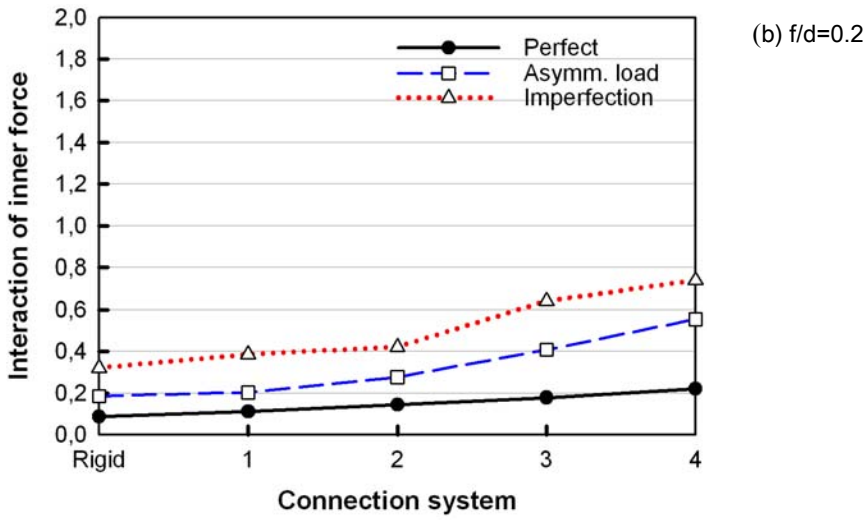
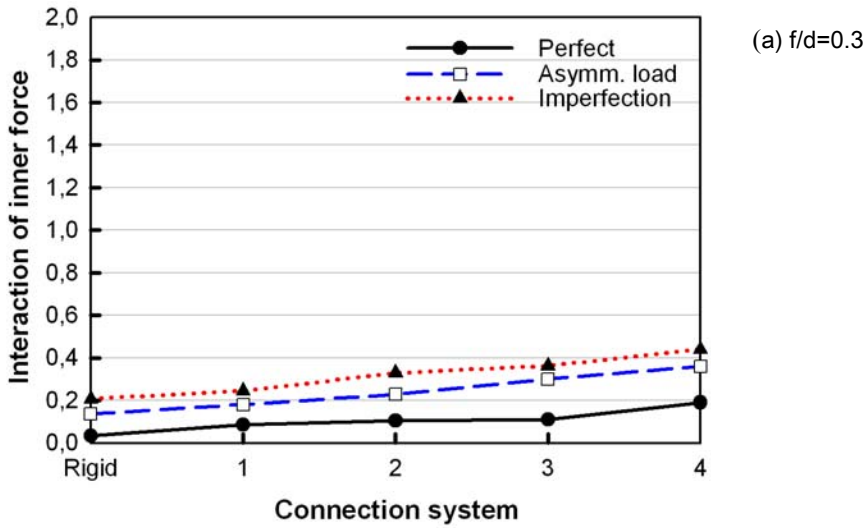


Figure 5.10:
Interaction of inner forces - f/d and various connection systems,
 $f=50$ m ($\Delta V=2.0$ mm)

Figure 5.7 and 5.9 show the failure load factors corresponding to f/d and four connection systems with the bolt clearance condition $\Delta V = 2.0$ mm, respectively. As shown in these figures, general failure load factors increase with the increment of the rise-span ratios and the connection system, which has a high nodal stiffness, and draws near to the failure load factor of the rigid connection system. The influence of connection stiffness with geometric initial imperfection shows clearly the high-rised shells. For example, the perfect system of 25 m shell in $f/d=0.3$ presents about 2.5 times higher failure load factor than the initial imperfection's one. In case of $f/d=0.1$, most of the models show a low failure load factor, and all of the models using systems 1 to 4 could not even reach design load level ($p=1$). General failure load factor of asymmetrical load case is a little bit higher than imperfection shape, but the models of $f/d=0.3$ with the connection systems 1,2,3 and 4 show almost similar failure load factors. In case of the grid shells of span 50 m, although the results of failure load factors are somewhat higher than the one of 25 m, general tendency is almost the same as 25 m grid shells.

Figure 5.8 and 5.10 show the interaction of internal member forces of each model obtained by formular 5.1. In the case of analysis models of 25 m, all in reveal member strengths of f/d 0.2 and 0.3 are in the safe ranges. However, in the case of f/d 0.1 shows that an asymmetric load with connection system 3 and 4, and the model of imperfection from first eigenform are at fail. The models of 50 m present s similar tendency as the models using 25 m. Only the model of 50-50-5 with the connection system 4 could not be sufficient for member strength. These phenomena predict that the model of 50 m consist of more members than the 25 m model, which leads to more sufficient member strength on the global structure. This parameter study also shows that the failure load is very strongly influenced by the geometrical initial imperfection.

The low failure load factor obtained by a combination of low stiffness of connection systems and initial imperfection in a low rise-span ratio can also be observed in the stress distribution. Figure 5.11~5.14 present the distributi-

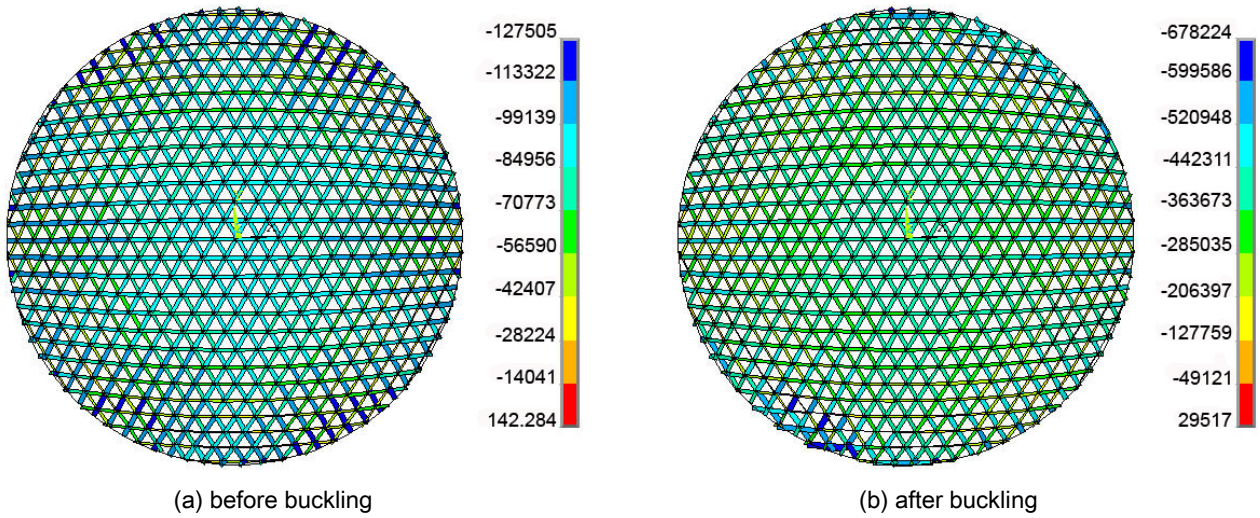


Figure 5.11:
Member forces with perfect shape (unit: N) - 25-25-5 ($f/d=0.2$) with connection system 4 ($\Delta V=2.0$ mm)

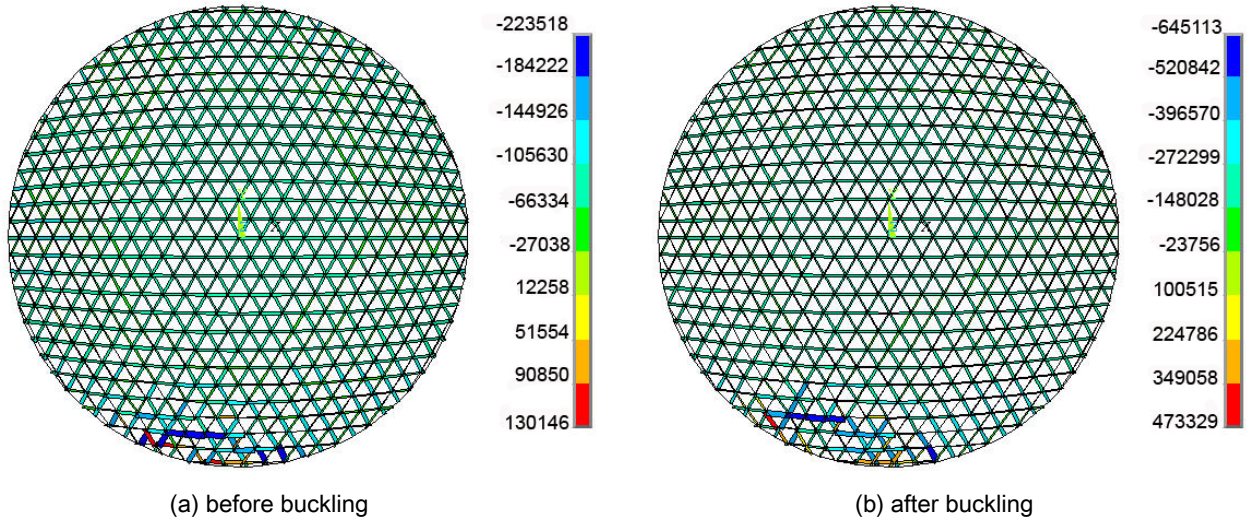


Figure 5.12:
Member forces with imperfection shape (unit: N) - 25-25-5 ($f/d=0.2$) with connection system 4 ($\Delta V=2.0$ mm)

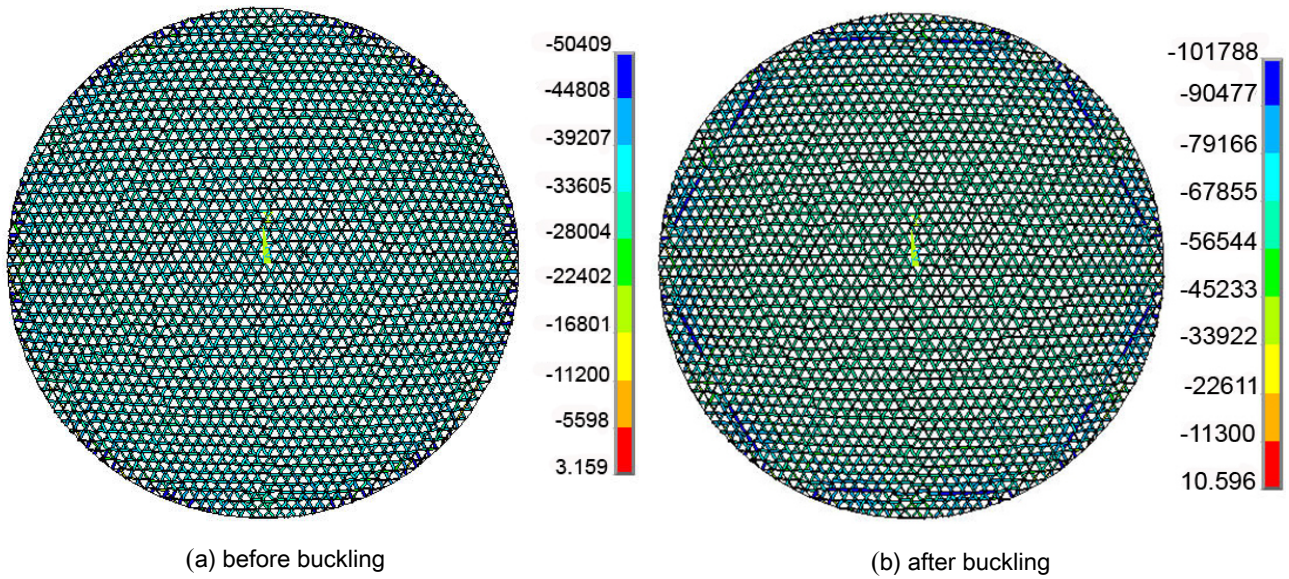


Figure 5.13:
Member forces with perfect shape (unit: N) - 50-50-5 ($f/d=0.1$) with connection system 4 ($\Delta V=2.0$ mm)

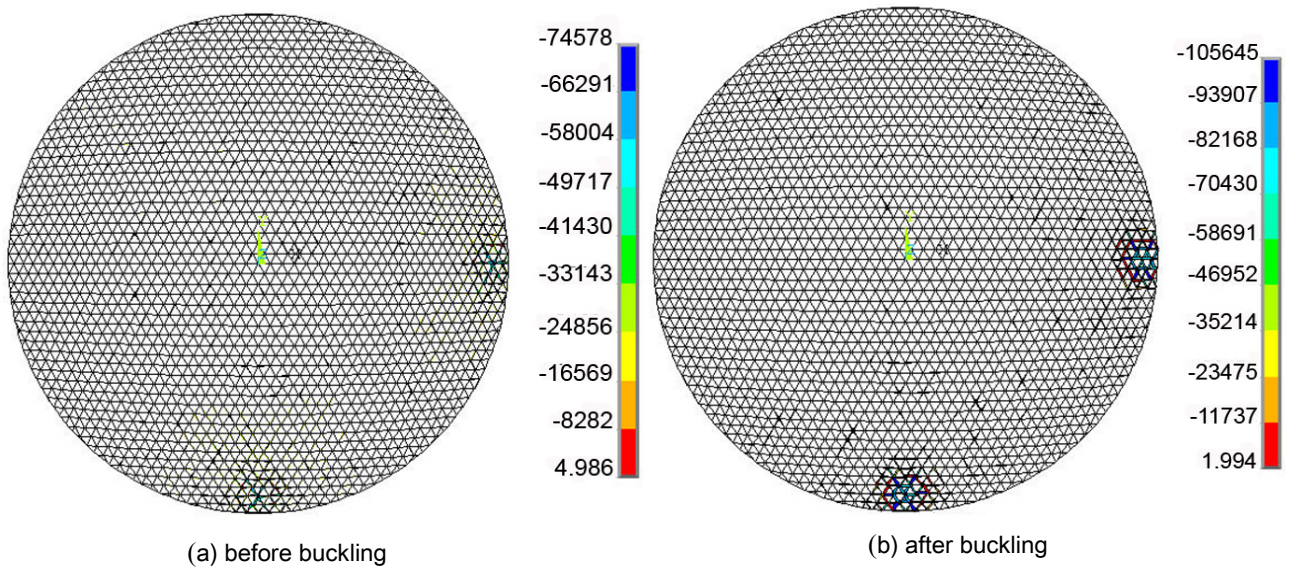


Figure 5.14:
Member forces with imperfection shape (unit: N)-50-50-5 ($f/d=0.1$) with connection system 4 ($\Delta V=2.0$ mm)

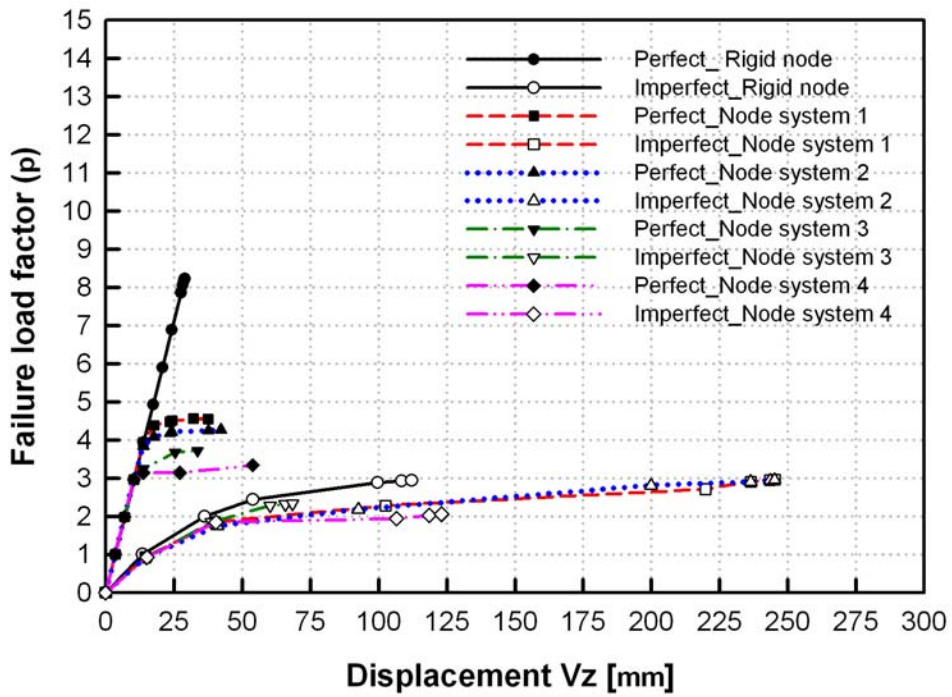


Figure 5.15:
Failure load factor-displacement curves of grid shell - 25-25-5 ($f/d=0.2$) ($\Delta V=2.0$ mm), g+s

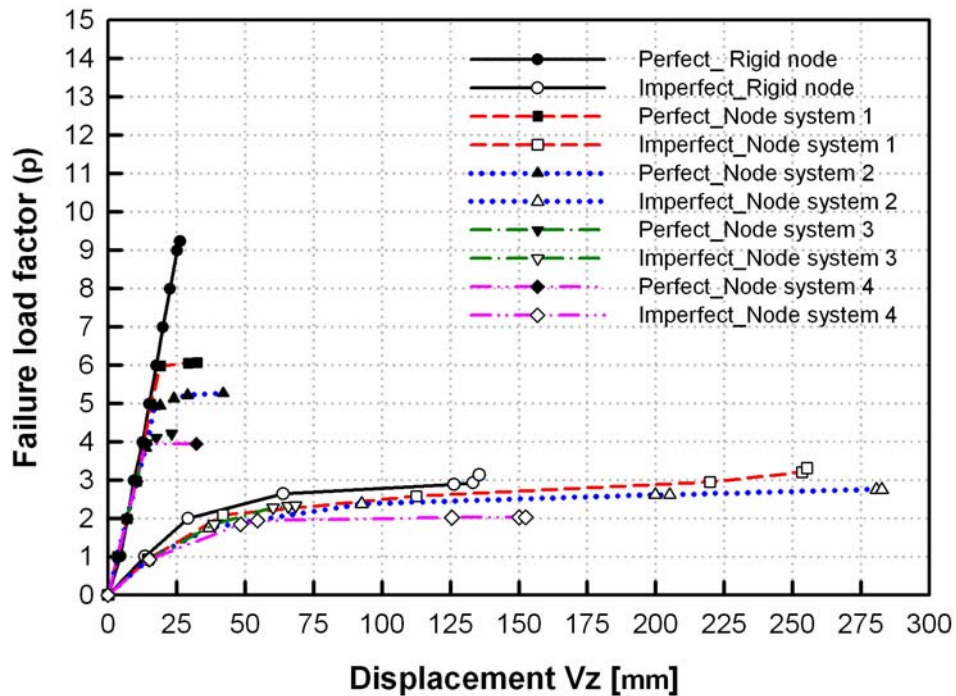


Figure 5.16:
Failure load factor-displacement curves of grid shell - 50-50-10 ($f/d=0.2$) ($\Delta V=2.0$ mm), g+s

ons of member forces. In the case of a perfect system, the distribution of member forces are almost uniform even with buckling phenomenon. However, the grid shell with the initial imperfection shows the non-uniform distribution of member forces even at the early phase of incremental load. Therefore, it can be observed that non-uniform stress occurs easily in the model by increasing external force, thus geometric initial imperfection of the grid shell along with a low stiffness of connection type in a low rise-span ratio causes the membrane stress to switch to bending stress easily, leading to the buckling behavior shown in the grid shell.

Figure 5.15 and 5.16 show the load-displacement behavior of the grid shell $f/d=0.2$ of 25 m and 50 m, respectively. For the perfect model, the failure load arrived at the critical point, i.e. where the tangent stiffness matrix turns singular. However, the failure load factor of imperfection models were reached either by a sudden plunge of the displacements or by the exceeding of member strength. In this case, the critical point where the singular point of tangent stiffness matrix could not be adopted as a failure load factor level. Hence, to catch the failure load factor for this case, the author had to look at the load-displacement curves and find out the load level where buckling is initiated. In case of $f/d=0.2$, membrane stress was changed easily to bending stress with the low connection stiffness in the initial imperfection. However, even with the low connection stiffness the perfect shape of the high-rised model such as $f/d=0.2$ showed a certain buckling path of form-resistance. As shown in Figure 5.15, for instance, the failure load factor of perfect shape with the weakest system 4 increases until factor 3 before the bifurcation occurred in the model. The cases of $f/d=0.3$ were also similar because the load carrying capacity increased when the rise of the grid shell becomes high. This buckling mode can explain that the critical point of the high-rised perfect grid shell with semi-rigid connection typically tend to a bifurcation point, where the final failure mode becomes quite different from the pre-buckling displacements, because its load-displacement path changes very suddenly to another buckling path at the crucial buckling point .

On the other hand, the model considered to initial imperfection shows a different failure load factor-displacement curve. In the case of 50-50-10, as shown in Figure 5.16, most analysis models reached design load factor ($p=1$) at least. However, the stiffness curves are very low of imperfection analysis, for instance the imperfect shape with connection system 4 reached at the load factor 1 with the displacement 12.7 mm, while the perfect one attained the load factor 4 with the displacement 10.8 mm. The reason for this phenomenon can be explained by only one load-displacement path and thus the pre- and post-critical buckling path which was caused by geometrical imperfection and thus the pre- and post-critical buckling path are almost identical. This results in a low form-resistance of global shell (Figure 5.16).

The distributions of the simulation's displacement with the models 25-25-7.5 ($f/d=0.3$) and 50-50-5 ($f/d=0.1$) show through Figure 5.17 to 5.20. To represent the diverse deformation mode, the connection system 2 with perfect and imperfection shapes of the model 25-25-7.5 and perfect and

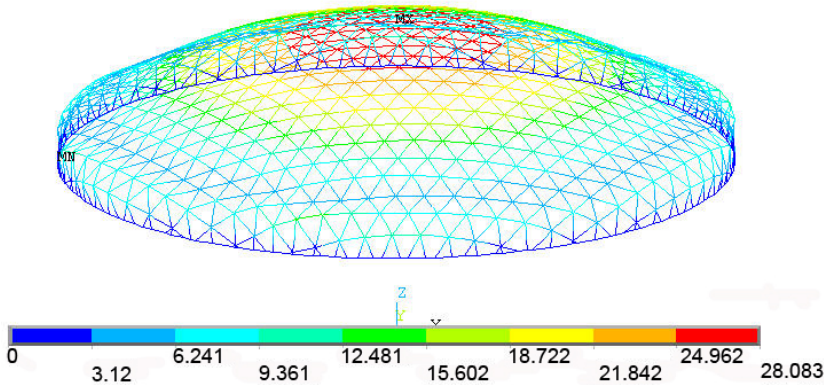


Figure 5.17:
Average displacement of perfect model 25-25-7.5 with connection system 2 ($\Delta V=2.0\text{mm}$), g+s (mm),

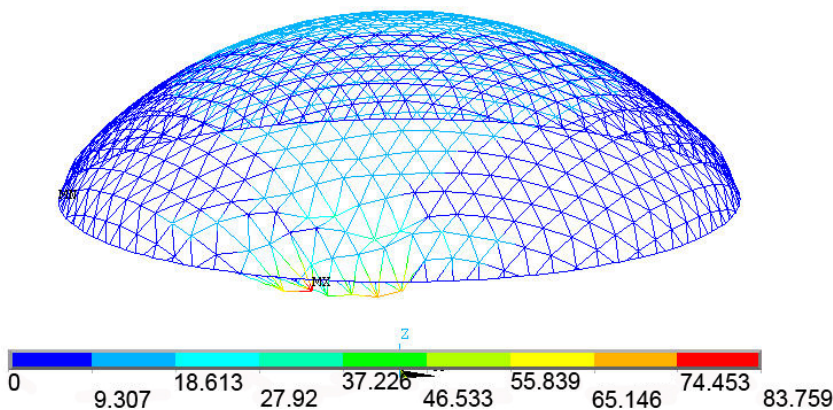


Figure 5.18:
Average displacement of imperfect model 25-25-7.5 with connection system 2 ($\Delta V=2.0\text{mm}$), g+s (mm)

imperfection shapes of the model 50-50-5 with the connection system 4 are shown. The corresponding deformations were up to the incremented load factor before buckling occurred. Due to the high connection stiffness and high rise-span ratio, the perfect model of 25-25-7.5 ($f/d=0.3$) is deformed as a strong global deformation (Figure 5.17). Even though the same model with an imperfection shape collapsed as a local deformation, the process of buckling can predict that the form of shell resisted somewhat until membrane force changed to bending force (Figure 5.18).

On the other hand, in the case of 50-50-5 ($f/d=0.1$) with connection system 4, shows different contours of deformation. Figure 5.19 presents the deformation of the perfect model. Because the model consists of a low rise-span with weak connection stiffness the form-resistance of shell is not so strong as $f/d=0.2$ or 0.3 , even with perfect shape, so the tendency of deformation is to head for a more or less local one. But the overall deformation can still be seen as a global deformation.

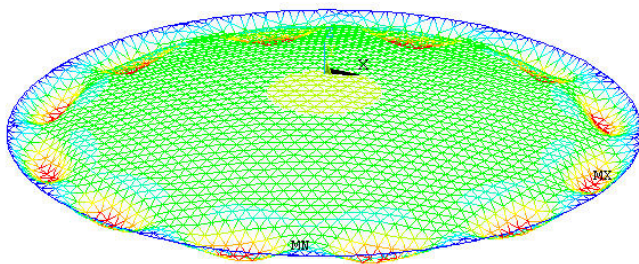


Figure 5.19:
Average displacement of perfect model 50-50-5 with connection system 4 ($\Delta V=2.0\text{mm}$), g+s (mm)

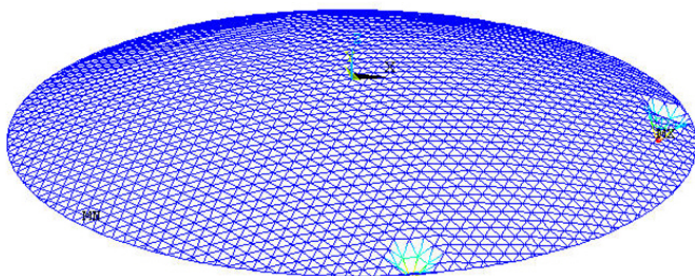
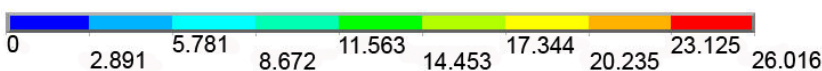
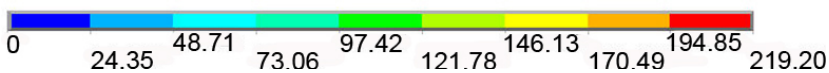


Figure 5.20:
Average displacement of imperfection model 50-50-5 with connection system 4 ($\Delta V=2.0\text{mm}$), g+s (mm)



The imperfection model of 50-50-5 with connection system 4 shows a typical local failure. The average displacement went to around 220 mm, local failures almost occurred and critical failure was gained very easily. That means that the form-resistance could not be obtained with the conditions of this model. This phenomenon also conveys how sensitively the failure load factor is influenced by low-rised imperfection shell with a connection system that has a low stiffness (Figure 5.20).

Concerning the buckling load of an asymmetrical load case, general failure load factors are higher than the imperfection shape based on 1st eigenmode, for example asymmetrical load case in the model 25-25-5 with connection system 2 showed about 34 % higher failure load factor than the imperfection. However, in the case of a low-rised model, such as 25-25-2.5 ($f/d=0.1$) with connection system 4, presented almost the same low failure load factor ($p=0.55$) between $g+s/2$ and imperfection, because the form-resistance or the spatial load transfer in this model are very weak due to the low rise-span ratio with the low stiffness of connection system. That caused a low failure load factor with large displacement (Figure 5.21).

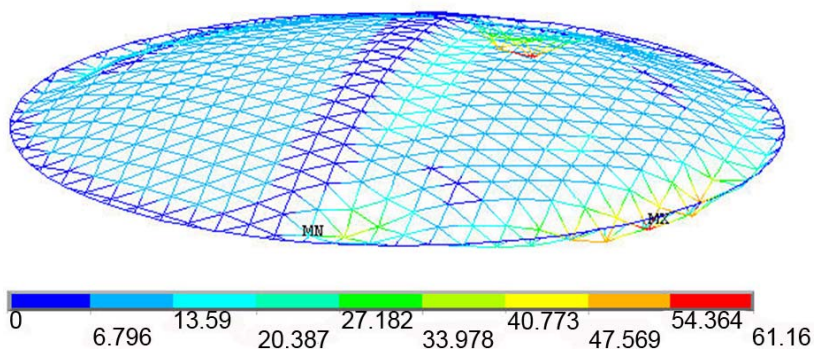


Figure 5.21:
Average displacement (mm) at failure load factor of grid shell 25-25-2.5 with connection system 4 ($\Delta V=2.0\text{mm}$), $g+s/2$ (mm)

5.5.2 The influence of different bolt clearances in the connection system with various rise-span on buckling load

In order to observe the influence of different bolt clearances in connection with various rise-span ratios on the buckling load of global grid shells, numerical buckling simulations were performed. The test models were already introduced in Table 5.1 and 5.2. All of the moment-rotation curves and load-displacement curves pertaining to bolt clearance 0.1 mm and 2.0 mm could be converted to the nonlinear spring element COMBIN39 from a specific element function of ANSYS as already presented in the last section.

In the Figure 5.22 to 5.25, the curves of failure load factors and average node displacement of analysis models are shown. To represent their specific characteristics bolt clearances with the various rise-span global grid shells, the models of 25-25-2.5 ($f/d=0.1$), 25-25-7.5 ($f/d=0.3$), 50-50-5 ($f/d=0.1$) and 50-50-15 ($f/d=0.3$) with connection systems 2 and 4 are introduced, respectively. As shown in chapter 4, system 2 retains a high connection stiffness of each M_y , M_z and F and, especially this system shows more clearly different curves than other systems according to the different bolt clearances. System 4 has a relative low stiffness with an obvious difference of axial forces (F) based on $\Delta V=0.1$ and 2.0 mm.

5.5.2.1 High-rise grid shell with various bolt clearances

As shown in Figure 5.22 and 5.23, with the high-rise model such as $f/d=0.3$, more obvious differences in failure load factors could be observed by connection system 2 than with the model using system 4. In the case of connection system 2, the failure load factor of $\Delta V=0.1$ mm of the perfect shape model is 9.8 while the case of bolt clearance 2.0 mm reached 8.85. The asymmetrical one shows a similar deviation of factor 0.92 between $\Delta V=0.1$ mm and 0.2 mm, and the imperfection model presents a factor 0.62 difference.

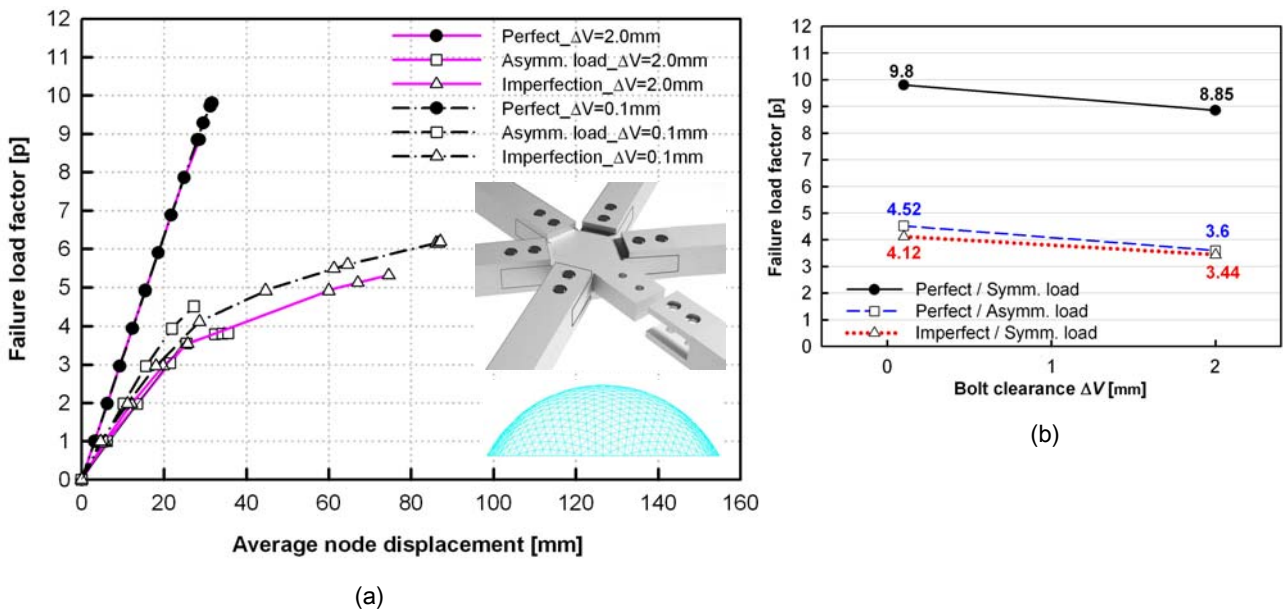


Figure: 5.22

Failure load factor-displacement curves - 25-25-7.5 ($f/d=0.3$) with the connection system 2 ($\Delta V=0.1\text{mm}$ and 2.0mm) (a) and comparing to failure load factors between different bolt clearances (b)

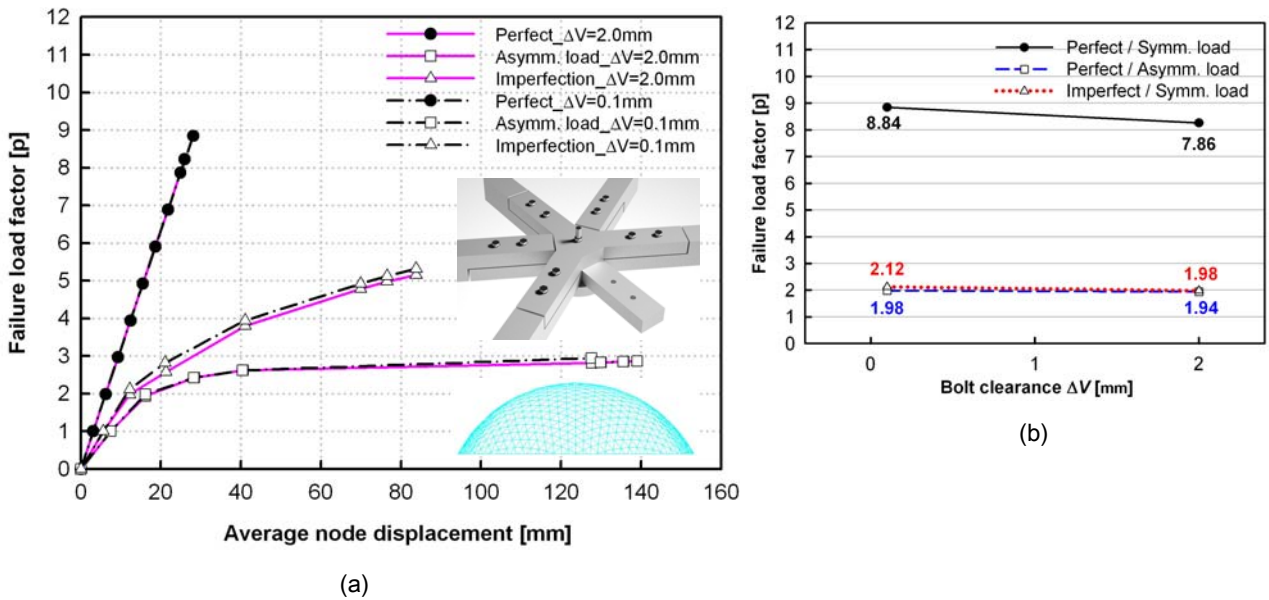


Figure 5.23:

Failure load factor-displacement curves - 25-25-7.5 ($f/d=0.3$) with the connection system 4 ($\Delta V=0.1\text{mm}$ and 2.0mm) (a) and comparing to failure load factors between different bolt clearances (b)

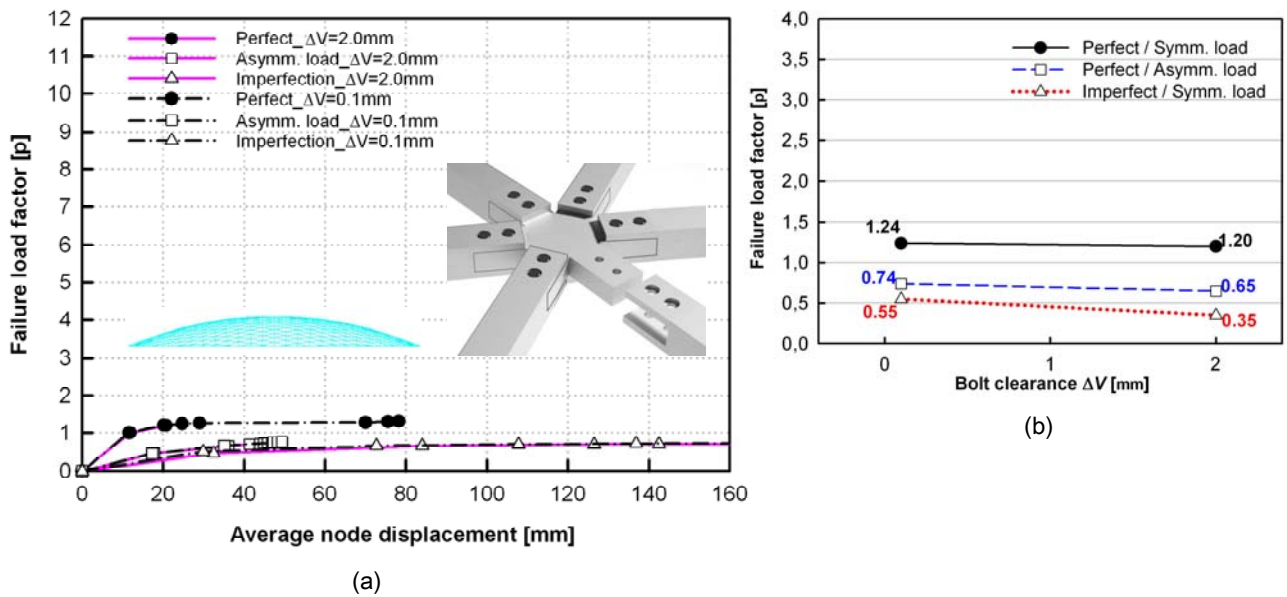


Figure 5.24: Failure load factor-displacement curves - 25-25-2.5 ($f/d=0.1$) with the connection system 2 ($\Delta V=0.1$ mm and 2.0mm) (a) and comparing to failure load factors between different bolt clearances (b)

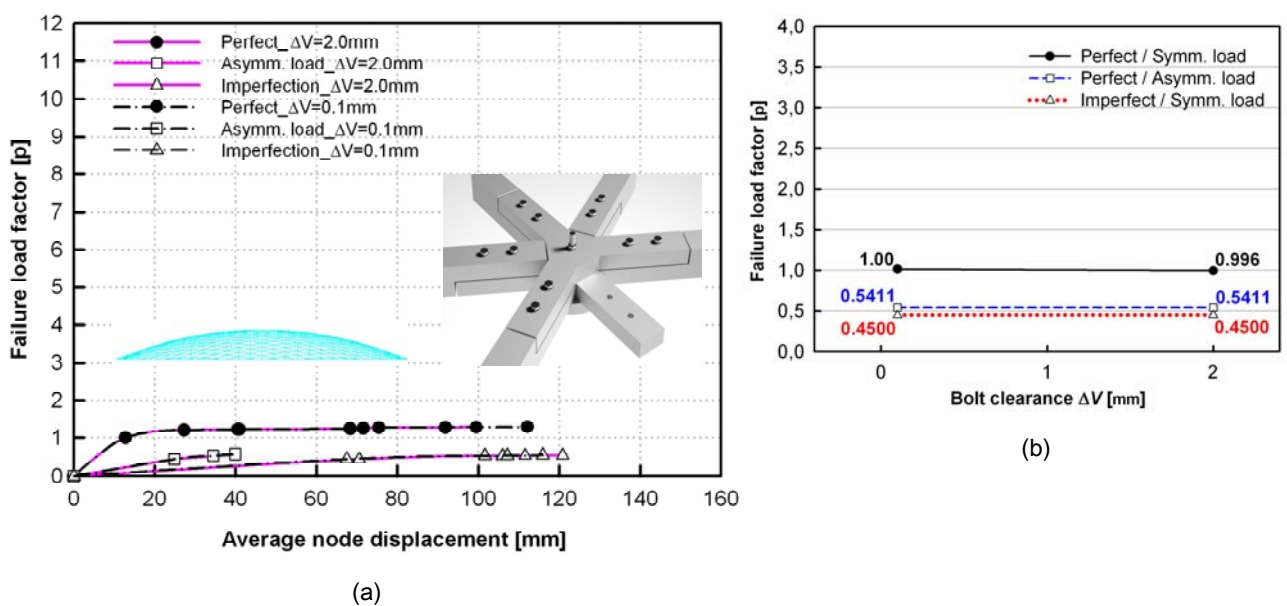


Figure 5.25: Failure load factor-displacement curves - 25-25-2.5 ($f/d=0.1$) with the connection system 4 ($\Delta V=0.1$ mm and 2.0mm) (a) and comparing to failure load factors between different bolt clearances (b)

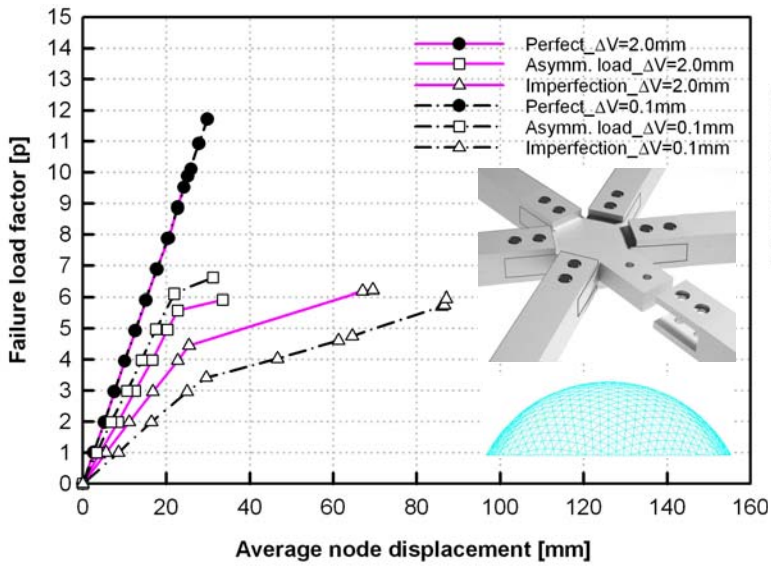
As for the high-rised long span model of 50-50-15, the differences of failure load factors with connection system 2 are shown as 1.6 for perfect shape, 0.73 for asymmetrical load and 1.04 for imperfection shape, respectively (Figure 5.26).

System 4, on the other hand, demonstrates some different behaviors on $f/d=0.3$. In 25 m and 50 m the gap of failure load factor of perfect shape between $\Delta V=0.1$ mm and 2.0 mm is also around factor 0.99. The critical points of asymmetrical load and imperfection shape applied different bolt clearances, this shows a smaller difference than the case with system 2, namely 0.14 and 0.04 for the model 25-25-7.5 and 0.02 and 0.21 for the model 50-50-15, respectively.

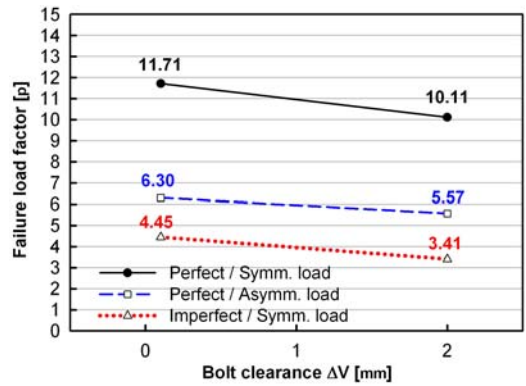
5.5.2.2 Low-rise grid shell with various bolt clearances

In terms of the low-rised model, such as 25-25-2.5 and 50-50-5 with the influence of bolt clearances, each of the failure load factor-displacement curves and the deviations of failure load factors based on different bolt clearances 0.1 mm and 2.0 mm are presented in this section. At first, in the case of 25-25-2.5, the perfect model with connection system 2 just shows a 0.13 differing factor, and the cases of asymmetrical load and imperfection shape just present 0.09 and 0.20 deviations, respectively (Figure 5.24). Figure 5.25 shows the same analysis model with connection system 4 and only the perfect model has a different value of 0.004 and the rest of the models such as asymmetrical load case and imperfection shape have little difference of failure load factor.

And these phenomena are similar to the values of model 50-50-5.0. As shown in Figure 5.28(b), the perfect model with system 2 had a different factor 0.1, and the deviations of asymmetrical load case and imperfection model between $\Delta V=0.1$ mm and 2.0 mm were 0.02 and 0.21, respectively. As for the same grid shell with connection system 4, except for the perfect model, the failure load factors of asymmetrical load and imperfection were the same (Figure 5.29).



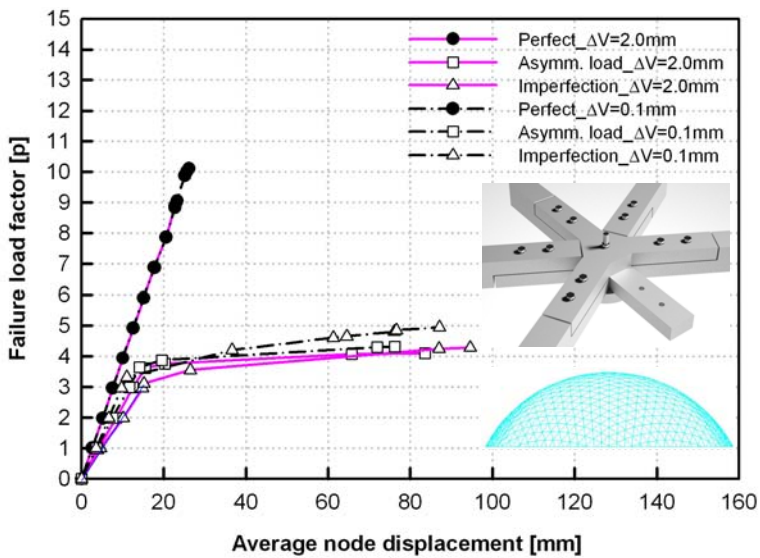
(a)



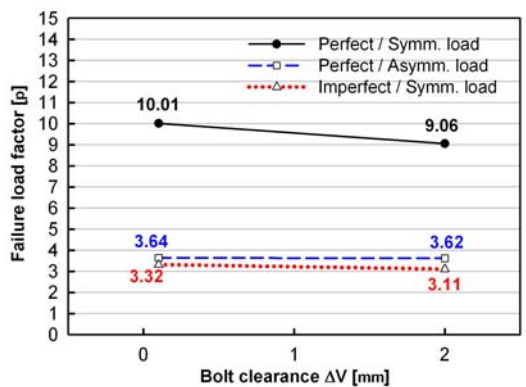
(b)

Figure 5.26:

Failure load factor-displacement curves - 50-50-15 ($f/d=0.3$) with the connection system 2 ($\Delta V=0.1\text{mm}$ and 2.0mm) (a) and comparing to failure load factors between different bolt clearances (b)



(a)



(b)

Figure 5.27:

Failure load factor-displacement curves - 50-50-15 ($f/d=0.3$) with the connection system 4 ($\Delta V=0.1\text{mm}$ and 2.0mm) (a) and comparing to failure load factors between different bolt clearances (b)

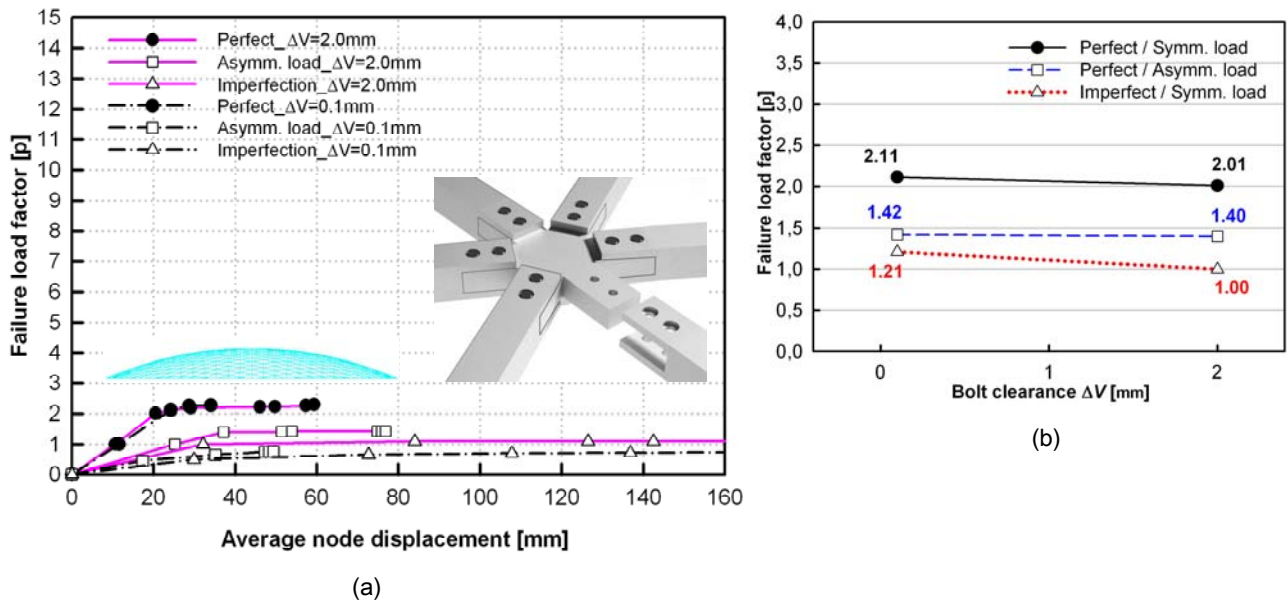


Figure 5.28: Failure load factor-displacement curves - 50-50-5.0 ($f/d=0.1$) with the connection system 2 ($\Delta V=0.1$ mm and 2.0 mm) (a) and comparing to failure load factors between different bolt clearances (b)

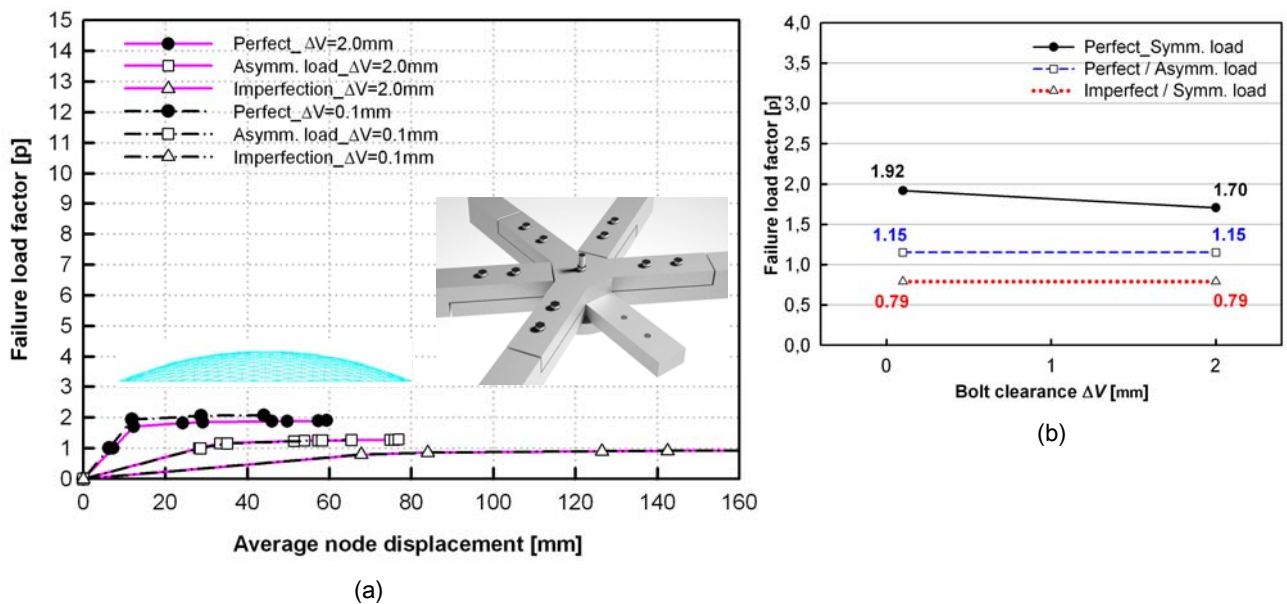


Figure 5.29: Failure load factor-displacement curves - 50-50-5.0 ($f/d=0.1$) with the connection system 4 ($\Delta V=0.1$ mm and 2.0mm) (a) and comparing to failure load factors between different bolt clearances (b)

As may be expected, these phenomena could explain that a general spatial load transfer of the low rise-span is usually weak, so that each node could not take load transfer to maintain the form-resistance in the grid shell. Therefore, the different connection stiffness due to various bolt clearances may not play a significant roll on the buckling load.

In the case of the high-rised model, the influence of various nodal stiffness based on different bolt clearances could be more clearly observed than on the low rise one, because the interactions of each member on the structure for the load transfer is higher than the low-rised grid shell. Thus, different stiffness from bolt clearances could be effected by the interactions of member forces such as M_y , M_z and F . For example, the high-rised models 25-25-7.5 and 50-50-15 in connection system 2 provide almost 10% and 14% differing factors between $\Delta V=0.1$ mm and 2.0 mm, because the rotational elastic bending capacity of $\Delta V=0.1$ mm in system 2 is around 33% higher than $\Delta V=2.0$ mm and the rotational elastic capacity of the connection stiffness of axial force (F) in $\Delta V=2.0$ mm is about 60% weaker than the one of $\Delta V=0.1$ mm.

As for connection system 4, which has almost no differing stiffness between bending moment but is comprised of a different stiffness of F , the perfect shape of the shell shows different failure load factors between $\Delta V=0.1$ mm and 2.0 mm as opposed to the one in system 2. However, even though a high-rise shell was performed, the failure load factor of $\Delta V=0.1$ mm with imperfection shape and asymmetrical load case $g+s/2$, which are mainly dominant with bending stress, shows almost the same values, because the bending stiffness M_y and M_z between $\Delta V=0.1$ mm and 2.0 mm of system 4 are almost the same.

In order to observe the interactions of each connection force with various rise-span ratios under the buckling load in detail, several axial force-load factor curves and moment-load factor curves are pre-

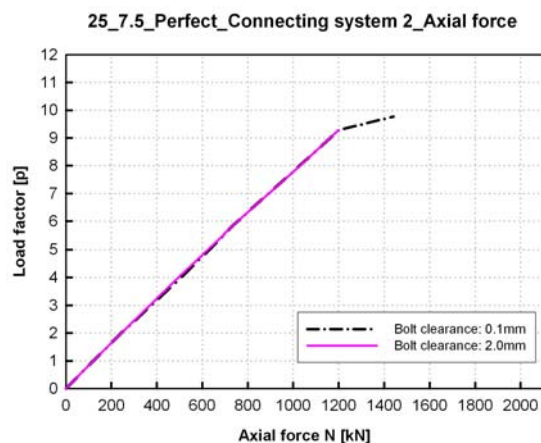


Figure 5.30: Max. axial forces in the perfect model 25-25-7.5 with the connection system 2 due to $\Delta V=0.1$ mm and 2.0mm.

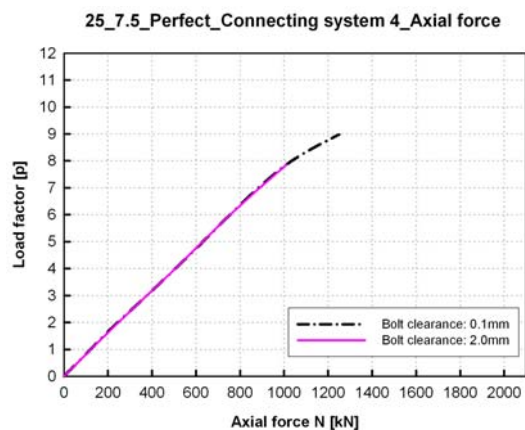


Figure 5.31: Max. axial forces in the perfect model 25-25-7.5 with the connection system 4 due to $\Delta V=0.1$ mm and 2.0mm.

sented as well (Figure 5.30 ~ 5.34). As shown in Figure 5.30 and 5.31, high-rised perfect models with connection system 2 and 4 show clear deviations of load factors although the paths of loading transfer are similar in each models. Figure 5.32 and 5.33 show load factors-bending moment M_y curves with the perfect model, asymmetrical load and imperfection models of the simulation model 25-25-7.5, which the patterns of load factor distinguished. In the case of the model in connection system 2, the values of M_y bolt clearances in the perfect model have the same load factor until the moment of M_y is 2.0 kNm. After that, M_y of $\Delta V=0.1$ mm increases to 3.4 kNm at the load factor 9.8. For the imperfection model, the bolt clearance 0.1 mm in this connection system shows about 10% higher stiffness than the one of bolt clearance 2.0 mm. The load factor of asymmetrical load case in the bolt clearance 0.2 mm just remained at load factor level 3 while the value of bolt clearance 0.1 rised to load factor level 4, due to the higher connection stiffness of $\Delta V=0.1$ mm rather than $\Delta V=2.0$ mm (Figure 5.32).

On the other hand, the same analysis model in connection system 4 provides different patterns in system 2. As the case of system 2 occurred, the perfect model with bolt clearances 0.1 mm and 0.2 mm of system 4 soared together until load factor 8.0 at the moment 1.35 kNm. After that, bolt clearance 0.1 mm went up to load factor 8.84 which was around factor 0.6 more than the value of bolt clearance 2.0 mm. However, the values of imperfection model and asymmetrical load case show very small differences between bolt clearance 0.1 mm and 2.0 mm, because connection system 4 shows very small difference of connection stiffness behaviors for bending moment between bolt clearances 0.1 mm and 2.0 mm by itself (Figure 5.33).

Figure 5.34 represents the patterns of M_y in the

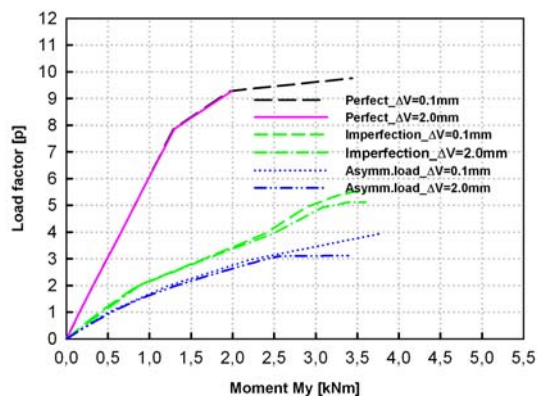


Figure 5.32:
Max. bending moments in the model 25-25-7.5 with the connection system 2 due to $\Delta V=0.1$ mm and 2.0mm.

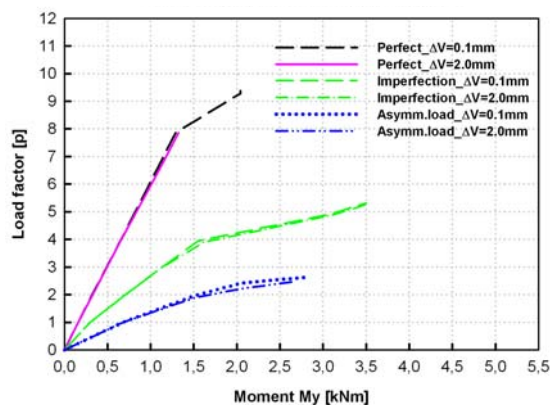


Figure 5.33:
Max. bending moments in the model 25-25-7.5 with the connection system 4 due to $\Delta V=0.1$ mm and 2.0mm.

low rise analysis model 25-25-2.5 with connection system 2 which showed an obviously different buckling load in the rise ratio $f/d=0.3$ (25-25-7.5) due to different bolt clearances. As shown in this figure, although connection system 2 contains various connection stiffness according to bolt clearances, the values of M_y in all cases provide very small different force interaction patterns between $\Delta V=0.1$ mm and 2.0 mm. It represents that the low rise grid shell is not so much influenced even by the connection system which contains different connection stiffness due to various bolt clearances. These phenomena are almost the same in the case of 50 m.

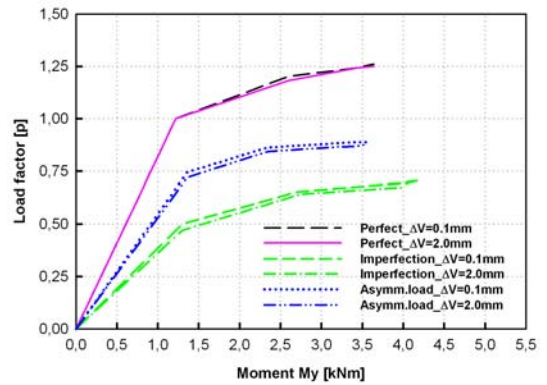


Figure 5.34:
Max. bending moments in the model 25-25-2.5 with the connection system 2 due to $\Delta V=0.1$ mm and 2.0mm.

Table 5.3:

Failure load factors and displacement of grid shell 25m

d [m]	f [m]	Connection System								
7.5	Rigid			Perfect		Asymm.		Imper.		
		Failure load factor	10.8		8.30		4.9			
		Displacement [mm]	35.70		40.53		65.41			
		1	B.C. (ΔV) [mm]							
			0							
					Perfect		Asymm.		Imper.	
		Failure load factor	9.80		4.40		3.60			
		Displacement [mm]	31.66		31.44		33.22			
		2	B.C. (ΔV) [mm]							
			0.1			2.0				
					Perfect	Asymm.	Imper.	Perfect	Asymm.	Imper.
			Failure load factor	9.80	4.52	4.12	8.85	3.6	3.44	
	Displacement [mm]		31.65	21.95	28.61	30.23	23.52	25.75		
	3		B.C. (ΔV) [mm]							
		0.1			2.0					
				Perfect	Asymm.	Imper.	Perfect	Asymm.	Imper.	
		Failure load factor	9.58	3.82	3.56	8.64	3.51	3.10		
		Displacement [mm]	27.20	26.29	22.43	28.08	28.72	19.83		
		4	B.C. (ΔV) [mm]							
	0.1			2.0						
			Perfect	Asymm.	Imper.	Perfect	Asymm.	Imper.		
	Failure load factor		8.84	1.98	2.12	7.86	1.94	1.98		
	Displacement [mm]		28.08	16.09	12.23	24.90	16.11	18.11		
	25		Rigid			Perfect		Asymm.		Imper.
Failure load factor		8.06		5.80		2.30				
Displacement [mm]		28.29		35.03		53.96				
1		B.C. (ΔV) [mm]								
		0								
				Perfect		Asymm.		Imper.		
Failure load factor		4.50		2.86		1.90				
Displacement [mm]		13.78		25.14		39.92				
2		B.C. (ΔV) [mm]								
		0.1			2.0					
				Perfect	Asymm.	Imper.	Perfect	Asymm.	Imper.	
		Failure load factor		4.08	2.84	1.90	4.17	2.74	1.84	
		Displacement [mm]	13.77	21.72	22.04	12.15	23.72	18.56		
		3	B.C. (ΔV) [mm]							
0.1			2.0							
			Perfect	Asymm.	Imper.	Perfect	Asymm.	Imper.		
Failure load factor			3.79	2.52	1.85	4.0	2.47	1.83		
Displacement [mm]			12.21	25.88	18.74	13.77	26.67	38.81		
4			B.C. (ΔV) [mm]							
		0.1			2.0					
				Perfect	Asymm.	Imper.	Perfect	Asymm.	Imper.	
		Failure load factor	3.58	2.08	1.10	3.92	1.89	1.15		
		Displacement [mm]	11.47	16.98	15.55	13.82	15.30	15.15		
		2.5	Rigid			Perfect		Asymm.		Imper.
Failure load factor	3.10			1.10		0.84				
Displacement [mm]	14.32			16.61		48.60				
1	B.C. (ΔV) [mm]									
	0									
				Perfect		Asymm.		Imper.		
Failure load factor	1.21			0.90		0.56				
Displacement [mm]	19.32			48.28		36.36				
2	B.C. (ΔV) [mm]									
	0.1			2.0						
				Perfect	Asymm.	Imper.	Perfect	Asymm.	Imper.	
	Failure load factor			1.24	0.74	0.55	1.20	0.65	0.35	
	Displacement [mm]		24.70	35.14	29.89	20.84	36.18	32.43		
	3		B.C. (ΔV) [mm]							
0.1			2.0							
			Perfect	Asymm.	Imper.	Perfect	Asymm.	Imper.		
Failure load factor			1.10	0.55	0.65	1.19	0.70	0.34		
Displacement [mm]			12.02	20.27	54.77	11.99	17.84	59.53		
4			B.C. (ΔV) [mm]							
	0.1			2.0						
			Perfect	Asymm.	Imper.	Perfect	Asymm.	Imper.		
	Failure load factor		1.00	0.54	0.45	0.996	0.54	0.45		
	Displacement [mm]		12.77	34.46	67.46	12.78	34.48	70.55		

Table 5.4:

Failure load factors and displacement of grid shell 50m

d [m]	f [m]	Connection System										
		Perfect		Asymm.			Imper.					
50	15	Rigid	Failure load factor		13.81		10.22		5.41			
			Displacement [mm]		32.44		37.14		63.87			
			B.C. (ΔV) [mm]		0							
		1	Perfect		Asymm.			Imper.				
			Failure load factor		10.82		6.23		4.14			
			Displacement [mm]		29.98		28.22		34.82			
		2	B.C. (ΔV) [mm]		0.1		2.0					
			Perfect		Asymm.		Imper.		Perfect		Asymm.	
			Failure load factor		11.71		6.30		4.45		10.11	
		3	B.C. (ΔV) [mm]		0.1		2.0					
			Perfect		Asymm.		Imper.		Perfect		Asymm.	
			Failure load factor		10.54		5.82		4.19		9.84	
	4	B.C. (ΔV) [mm]		0.1		2.0						
		Perfect		Asymm.		Imper.		Perfect		Asymm.		
		Failure load factor		10.01		3.64		3.32		9.06		
	10	Rigid	Perfect		Asymm.			Imper.				
			Failure load factor		8.99		6.22		2.29			
			Displacement [mm]		25.30		33.63		29.25			
		1	B.C. (ΔV) [mm]		0							
			Perfect		Asymm.			Imper.				
			Failure load factor		6.06		3.92		2.08			
		2	B.C. (ΔV) [mm]		0.1		2.0					
			Perfect		Asymm.		Imper.		Perfect		Asymm.	
			Failure load factor		6.12		4.03		2.61		4.94	
		3	B.C. (ΔV) [mm]		0.1		2.0					
			Perfect		Asymm.		Imper.		Perfect		Asymm.	
			Failure load factor		4.50		3.18		1.94		4.45	
	4	B.C. (ΔV) [mm]		0.1		2.0						
		Perfect		Asymm.		Imper.		Perfect		Asymm.		
		Failure load factor		4.82		2.55		1.11		3.94		
	5.0	Rigid	Perfect		Asymm.			Imper.				
			Failure load factor		4.30		1.92		1.64			
			Displacement [mm]		12.75		16.62		41.55			
		1	B.C. (ΔV) [mm]		0							
			Perfect		Asymm.			Imper.				
			Failure load factor		2.71		1.50		1.26			
2		B.C. (ΔV) [mm]		0.1		2.0						
		Perfect		Asymm.		Imper.		Perfect		Asymm.		
		Failure load factor		2.11		1.42		1.21		2.01		
3		B.C. (ΔV) [mm]		0.1		2.0						
		Perfect		Asymm.		Imper.		Perfect		Asymm.		
		Failure load factor		1.99		1.45		0.97		1.99		
4	B.C. (ΔV) [mm]		0.1		2.0							
	Perfect		Asymm.		Imper.		Perfect		Asymm.			
	Failure load factor		1.92		1.15		0.79		1.70			

5.6 Summary

To predict the influence of buckling load on the global grid shell with various types of connection systems, FE-analysis of 25 m and 50 m three-way grid shells were simulated, in particular, taking differing bolt clearance sizes into consideration.

As for the influence of rise-span ratio and nodal stiffness on the buckling load, low connection stiffness with the imperfection model brings member stress to switch to bending stress easily, so that it decreases the failure load factor crucially. Maximum bending moment of the beam member at the failure load factor was identical with the maximum capacity of the connection system's bending moment. For instance, in all simulations with connection system 2, the maximum bending moment of the global loading test did not exceed the maximum bending capacity of connection system 2 (3.6 kNm).

In general, especially for the perfect models, it was found that some maximum axial force on the beam member was higher than their connection system's capacity of axial force at the failure load factor. This phenomenon could be explained by the membrane force transferring to the yield point of the member's material (355 N/mm^2) within the in-plane buckling capacity. Hence, it could be seen for the imperfection model that the bending moment capacity of connection system can determine the buckling load, which membrane stress changes into bending stress until failure mode occurs in the structure.

The influence of bolt clearances in the connection system on the buckling load for the global grid shells is dependent on the connection system and rise-span ratio. For example, in the high-rised perfect grid shell (25-25-7.5) with connection system 2, the failure load factor with $\Delta V=0.1 \text{ mm}$ obtained around 9.7% higher than $\Delta V=2.0 \text{ mm}$. System 4 with the same rise-span ratio model presented around 7% difference because the high-rise perfect grid shell is mainly influenced by compressive axial force until failure state and axial forces of both connection systems showed clearly different values of connection stiffness of axial load (F).

However, high-rised models based on the initial imperfection and asymmetrical load case showed slightly different results. In the case of the model 50-50-15 in connection system 2, for instance, $\Delta V=0.1$ mm of asymmetrical load case and initial imperfection one presented 11.6 % and 23.4 % higher than the values of $\Delta V=2.0$ mm. However, with the same grid shell model with connection system 4 showed just 0.55 % and 6.5 % deviations between $\Delta V=0.1$ mm and 2.0 mm, so that system 4 had very small difference in bolt clearances of 0.1 mm and 2.0 mm considering bending stiffness by itself.

Concerning the low-rise grid shell in 25-25-2.5, although system 2 showed somewhat differing values between $\Delta V=0.1$ mm and 2.0 mm, there were very small deviations of the overall failure load factors due to the low spatial load transfer in the global structure.